Ground Current Modification of Mobile Terminal Antennas and Its Effects

Md. Rashidul Islam, *Student Member, IEEE*, and Mohammod Ali, *Senior Member, IEEE*

***Abstract*—In this letter, a dual-band parasitic radiator is designed and optimized to modify the current distribution on the ground plane of a handheld terminal. Using a variable-length dual-band parasitic radiator, the ground current distribution is controlled, and low specific absorption rate (SAR) and high radiation efficiency at 900 and 1880 MHz are obtained. The proposed antenna scheme consisting of a dual-band parasitic element and a driven dual-band antenna reduces the peak SAR by 50% and 40% at 900 and 1880 MHz, respectively, compared to a conventional dual-band antenna. Significant increase in radiation efficiency is also obtained.**

***Index Terms*—Handset antenna, parasitic radiator, radiation efficiency, RF exposure, specific absorption rate (SAR).**

I. Introduction

RESEARCHERS are exploring new techniques to reduce the specific absorption rate (SAR) induced in a user's head or body by internal antennas used in mobile wireless devices. Techniques such as the use of a ferrite sheet [1], split-ring resonator [2], electromagnetic band-gap (EBG) structure [3], and engineered ground plane [4] have been reported. Implementing these techniques can be costly and complex. For example, the split-ring resonators proposed in [2] decrease the antenna gain and require additional space. The use of ferrites generally reduces the amount of radiated power.

In [5], a 45×40 mm^2 parasitic metal radiator was used on the back of a ground plane. It was shown that the peak SAR was reduced accompanied by higher radiation efficiency at 900 MHz. Placing a large metal radiator on a certain height in the back of a ground plane will increase the thickness of the device, which is undesirable. Ground plane extension in the form of two metal prongs was proposed to improve the radiation efficiency at the GSM 900-MHz and DCS 1800-MHz bands [6]. In [7], two L-shaped parasitic elements were placed on the front side of a ground plane to enhance the radiation efficiency at 2000 MHz. The authors in [8] showed that the near field due to a PCS 1900-MHz antenna could be controlled to improve the hearing aid compatibility (HAC) using two L-shaped parasitic radiators.

In this letter, a new technique is introduced where by designing and optimizing a dual-band parasitic radiator in the vicinity of a driven dual-band planar inverted-F antenna (PIFA), the current distributions on the ground plane can be significantly altered, both at 900 and at 1880 MHz. This helps us reduce the SAR at 900 and 1880 MHz and enhance the antenna radiation efficiency. SAR and radiation efficiency are studied when the proposed dual-band parasitic radiator along with a conventional dual-band driven PIFA is placed next to a homogeneous head phantom. The separation between the head and the ground plane containing the antenna was kept at 2 mm.

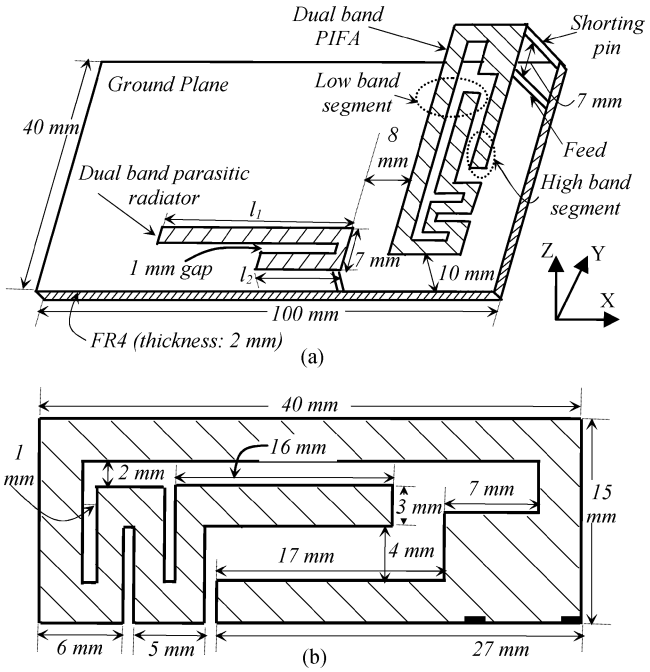

Fig. 1. (a) Proposed dual-band antenna geometry with the dual-band parasitic radiator. (b) Detailed dimensions of the driven dual-band antenna.

II. Proposed Antenna Geometry

The proposed geometry consisting of the dual-band parasitic element and a dual-band driven PIFA is shown in Fig. 1(a). The driven PIFA consists of a longer element responsible for the resonance at the low frequency band and a shorter element responsible for the resonance at the high frequency band. The antenna and the parasitic element were placed on a 100×40 mm^2 ground plane, underneath which was a 2-mm-thick FR4 substrate. There is no conductor on the bottom of the FR4 substrate. Detail dimensions of the driven PIFA are given in Fig. 1(b).

The dual-band parasitic element resembles an inverted-L antenna (ILA), except that it has two branches, l_1 and l_2 for 900 MHz (GSM 900 TX) and 1880 MHz (PCS 1900 TX), respectively. The separation between the parasitic ILA and the

Manuscript received in February 23, 2011; revised March 21, 2011; accepted April 15, 2011. Date of publication May 02, 2011; date of current version May 23, 2011.

The authors are with the University of South Carolina, Columbia, SC 29208 USA (e-mail: alimo@email.sc.edu).

Color versions of one or more of the figures in this letter are available online at http://ieeexplore.ieee.org.

Digital Object Identifier 10.1109/LAWP.2011.2149490

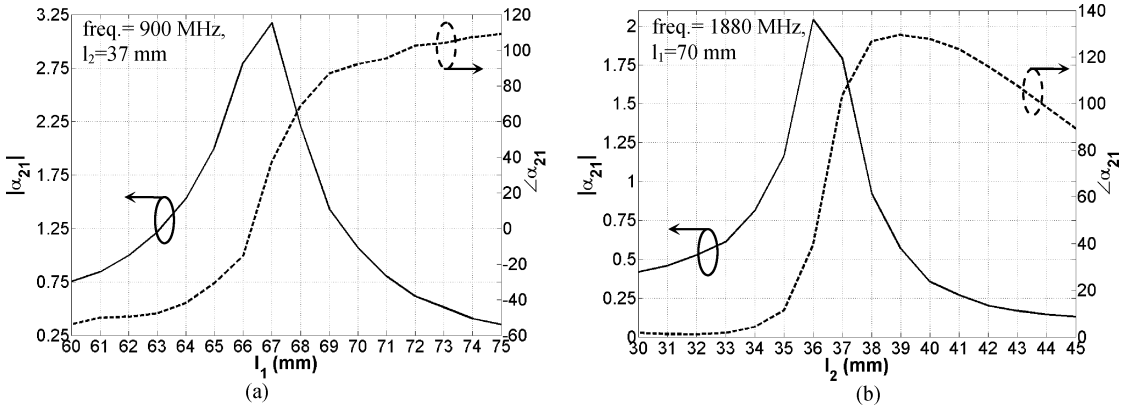

Fig. 2. Magnitude and phase of α_{21} in free space at (a) 900 MHz, $l_2 = 37$ mm and (b) 1880 MHz, $l_1 = 70$ mm.

driven PIFA was 8 mm [Fig. 1(a)]. This ensures a distance of 20 mm between the parasitic ILA and the high-band element of the driven PIFA for good impedance match [9]. The two metal strips of the parasitic ILA were 3 mm wide, and they were connected by a 2×1 mm^2 metal plate. Both the parasitic and driven antennas were at the same height (10 mm) from the ground plane.

Due to the vicinity of the driven PIFA to the parasitic ILA, it is expected that currents will be induced in the parasitic ILA both at 900 and 1880 MHz through electromagnetic coupling. In Section III, we determine the optimum lengths of l_1 and l_2 by analyzing the induced currents at the two frequencies.

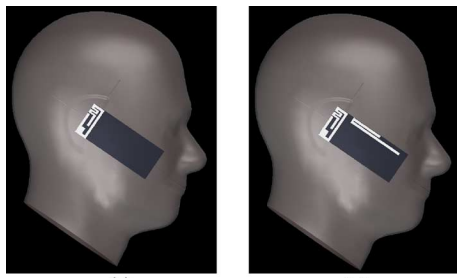

Fig. 3. PIFA against the head phantom (a) without and (b) with the parasitic ILA.

III. Analysis of Induced Currents

The impedance (Z) matrix that defines the voltages and currents in the driven and parasitic antennas is given in

$$\begin{bmatrix} V_1 \\ 0 \end{bmatrix} = \underbrace{\begin{bmatrix} Z_{11} & Z_{12} \\ Z_{21} & Z_{22} \end{bmatrix}}_{Z \text{ matrix}} \begin{bmatrix} I_1 \\ I_2 \end{bmatrix} \tag{1}$$

where the subscripts 1 and 2 correspond to the driven PIFA and the parasitic ILA, respectively. It is apparent that the Z_{NN} and the Z_{MN} are the self and mutual impedances in the Z matrix. The excitation voltage in the driven PIFA is V_1. Since the ILA is shorted to the ground plane, its feed-point voltage is zero. The ratio of the currents, α_{21}, can be expressed by

$$\alpha_{21} = \left(\frac{I_2}{I_1}\right) = \frac{-Z_{21}}{Z_{22}}. \tag{2}$$

The magnitude and phase of α_{21} in free space were calculated at 900 and 1880 MHz using HFSS [10]. In simulation, the shorting metal plate of the parasitic ILA was replaced by a lumped voltage source in order to compute the Z-parameters. In reality, the parasitic element will be shorted to the ground. Fig. 2(a) shows the magnitude and phase of α_{21} at 900 MHz for $l_2 = 37$ mm fixed (about a quarter-wavelength at 1880 MHz). In Fig. 2(a) l_1 varies from 60 to 75 mm. At 900 MHz, the maximum value for $|\alpha_{21}|$ occurs when $l_1 = 67$ mm. Note that at this point $\angle\alpha_{21}$ is not maximum. As l_1 increases further, $|\alpha_{21}|$ decreases, and $\angle\alpha_{21}$ increases and then saturates. It is expected that the point at which the largest $|\alpha_{21}|$ and $\angle\alpha_{21}$ occur will most likely be the point of interest (reduced SAR and higher antenna efficiency). This is so because a larger value of out-of-phase current in the parasitic ILA will strongly affect the current in the driven PIFA. With this in mind, we studied the SAR and radiation efficiency at 900 MHz by considering l_1 varying from 62 to 74 mm.

Fig. 2(b) shows the results at 1880 MHz, where l_2 was varied between 30 and 45 mm while l_1 was fixed at 70 mm (about quarter-wavelength at 900 MHz). Similarly to the case for 900 MHz, SAR and radiation efficiency were studied at 1880 MHz by varying l_2 from 32 to 44 mm because that is where $|\alpha_{21}|$ and $\angle\alpha_{21}$ intersect with each other.

IV. Results

A. SAR and Radiation Efficiency

SAR and radiation efficiency induced by a driven PIFA not containing any parasitic ILA were computed. A homogeneous human head phantom [specific anthropomorphic mannequin (SAM) [11]] was used. This scenario is illustrated in Fig. 3(a). The bottom surface of the 2-mm-thick FR4 board lying underneath the metal ground plane was touching the head [Fig. 3(a)]. Thus, the separation between the ground plane and the head was 2 mm. Next, the configuration shown in Fig. 1(a) was placed next to the SAM phantom. This scenario is illustrated in Fig. 3(b). SAR and radiation efficiency were computed using XFDTD [12]. These results are listed in Table I.

As is apparent, at 900 MHz the presence of the parasitic ILA significantly alters the peak 1-g and 10-g average SAR and the antenna efficiency. Compared to a conventional dual-

TABLE I
SAR AND RADIATION EFFICIENCY AT 900 AND 1880 MHZ DUE TO A DRIVEN DUAL-BAND PIFA WITHOUT ANY PARASITIC ELEMENTS AND WITH A DUAL-BAND PARASITIC ILA

Frequency	Antenna configurations		Peak 1-g avg. SAR (W/Kg)	Peak 10-g avg. SAR (W/Kg)	Radiation Efficiency
900 MHz, 250 mW	Driven PIFA without any parasitic elements		2.60	1.76	24.7%
	l_2=37 mm	l_1=62 mm	3.04	2.04	20.1%
		l_1=67 mm	1.95	1.31	36.6%
		l_1=68 mm	1.36	0.86	49.2%
		l_1=69 mm	1.29	0.88	47.5%
		l_1=70 mm	1.51	1.06	40.6%
		l_1=74 mm	2.10	1.42	30.6%
	l_1=68 mm, l_2=38 mm		1.36	0.86	49.3%
1880 MHz, 125 mW	Driven PIFA without any parasitic elements		1.77	0.97	48.8%
	l_1=70 mm	l_2= 32 mm	1.95	1.09	47.4%
		l_2=36 mm	2.09	1.23	43.8%
		l_2=37 mm	1.10	0.65	53.6%
		l_2=38 mm	1.13	0.62	55%
		l_2=44 mm	1.67	0.92	50.5%
	l_1=68 mm, l_2=38 mm		1.07	0.58	55.0%

band PIFA, the proposed technique results in significant SAR reduction (1.29 W/kg against 2.6 W/kg for 1-g average, and 0.88 W/kg against 1.76 W/kg for 10-g average). Antenna radiation efficiency increases from 24.7% to 49.2%. An interesting thing to note is that the SAR varies quite rapidly with variation in l_1, especially in the range of 67–70 mm. This is corroborated by the results shown in Fig. 2(a), where it also shows that $|\alpha_{21}|$ and $\angle\alpha_{21}$ vary quite rapidly when l_1 is in the range of 67–70 mm.

The lowest SAR was induced for $l_1 = 69$ mm. From Fig. 2(a), it is clear that the current magnitude is maximum for $l_1 = 67$ mm ($l_2 = 37$ mm). However, the phase of the current is not at its maximum for $l_1 = 67$ mm. As l_1 increases to 68 and 69 mm, the phase difference ($\angle\alpha_{21}$) starts increasing with a decreasing $|\alpha_{21}|$ value. Thus, lower SAR is obtained as long as both $|\alpha_{21}|$ and $\angle\alpha_{21}$ are high. Up to 50% reduction in both peak 1-g and 10-g average peak SAR is feasible (Table I). Conversely, when $l_1 = 62$ and 74 mm, both the 1-g and 10-g avg. SAR are higher. The last l_1, l_2 combination in the 900-MHz data in Table I correspond to that combination for which both SAR reduction and radiation efficiency at 900 and 1880 MHz are optimum.

Using Fig. 2(b), the 1880-MHz SAR data in Table I can be explained. As before, maximum SAR reduction is obtained when both $|\alpha_{21}|$ and $\angle\alpha_{21}$ are high. SAR reduction of as much as 40% is observed at 1880 MHz for $l_1 = 68$ mm, $l_2 = 38$ mm. Similarly as before for $l_2 = 32$ and 44 mm, SAR data are generally higher. Note that, in [8], the authors demonstrated a 23% reduction in peak SAR at 1880 MHz using two L-typed parasitic radiators.

The reduction in the peak SAR using the proposed technique can be explained with the help of the current distributions on the ground plane. Fig. 4(a) and (b) shows the ground plane current distributions at 900 MHz for the dual-band PIFA without the parasitic ILA and with the parasitic ILA ($l_1 = 68$ mm, $l_2 = 38$ mm), respectively. For clarity, current vectors only in certain portions are shown. It is clear that the parasitic ILA alters the currents on the ground plane [Fig. 4(b)] considerably. This leads to the reduction in the electromagnetic energy deposited in the head phantom and, hence, lower SAR. A similar reasoning can be applied for the ground plane currents induced at 1880 MHz.

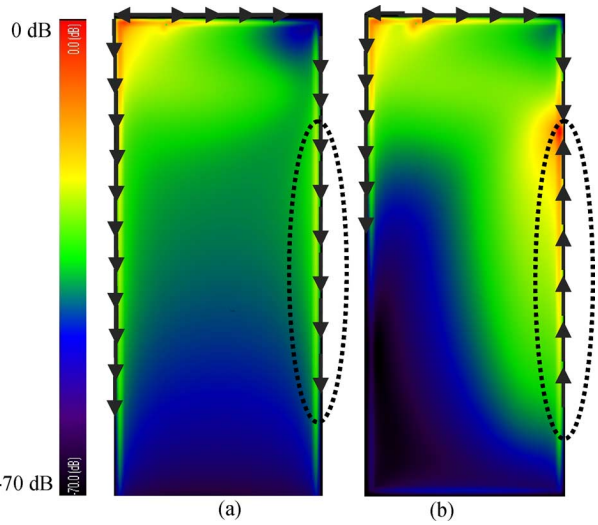

Fig. 4. Normalized current distribution on the ground plane at 900 MHz for PIFA against the head phantom (a) without and (b) with the parasitic ILA. Current vectors (not scaled to magnitudes) are shown for certain portions.

Another reason for the SAR reduction using the proposed scheme is the phase reversal of the current vectors in one of the two edges of the ground plane. As seen in Fig. 4(b), due to the presence of the parasitic ILA, the currents flowing at one of the edges of the ground plane oppose those at the other edge. As a result, near field becomes weaker, which contributes to lower SAR.

From Table I, the proposed configuration shown in Fig. 1(a) increases the radiation efficiency both at 900 and 1880 MHz. A twofold increase in the radiation efficiency can be achieved at 900 MHz. However, efficiency increase is only modest at 1880 MHz. This is because the ground plane radiates about 90% and 50% of the total radiated power at 900 and 1880 MHz, respectively [13]. As a consequence, more energy is coupled from the ground plane to the parasitic ILA at 900 MHz. Thus, the improvement in radiation efficiency is higher at 900 MHz with the parasitic ILA.

When the proposed antenna geometry was placed on the other side of the SAM phantom (touching the left ear spacer), similar performance improvements were observed. For example, at 900 MHz, the peak average SAR reduced by 52% and antenna efficiency increased from 25.8% to 50% for $l_1 = 68$ mm, $l_2 = 38$ mm.

B. *Free-Space S_{11} Results*

First, the dual-band PIFA without any parasitic ILA [shown in Fig. 1(b)] was designed for operation at the GSM 900 (880–960 MHz) and PCS 1900 (1850–1990 MHz) frequency bands. Second, the dual-band ILA was added. Fig. 5 shows computed (XFDTD) free-space S_{11} (dB) data for the first and second cases. Measured data are also shown for these cases.

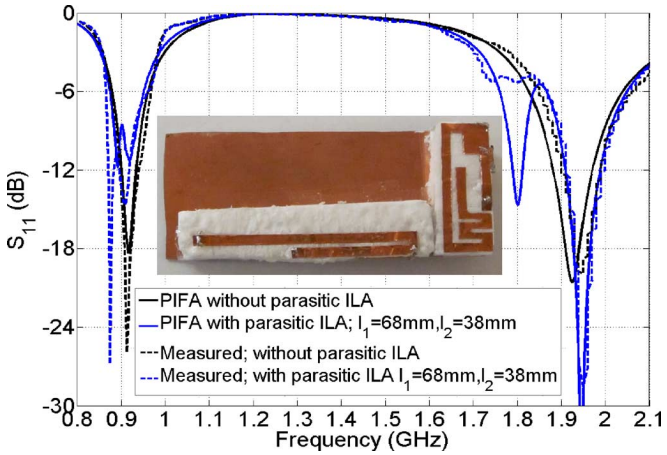

Fig. 5. Free space S_{11} data of the dual band PIFA without and with the parasitic ILA.

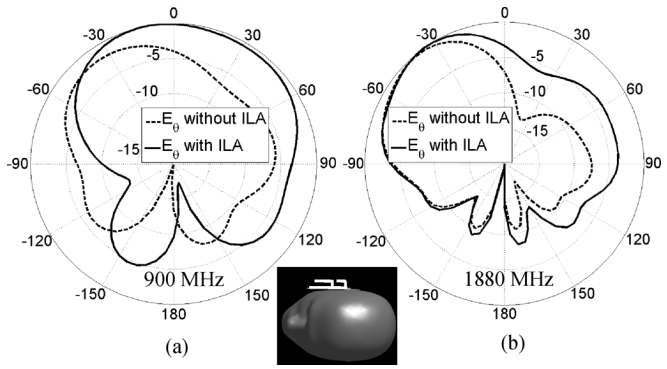

Fig. 6. Computed radiation patterns of the dual-band PIFA with and without the parasitic ILA. $l_1 = 68$ mm, $l_2 = 38$ mm. E_θ in the $\varphi = 0°$ plane.

For the parasitic ILA, $l_1 = 68$ mm and $l_2 = 38$ mm were used. The dual-band PIFA without the parasitic ILA (black solid line) has bandwidths of 80 and 210 MHz in the low and high bands, respectively, with $S_{11} <= -6$ dB. Measured data without the ILA (black dashed line) agree well with the computed data. When the parasitic ILA was added, additional resonances occurred. Measured data in this case are also in good agreement with the computed data. A small discrepancy can be seen in the high band, which is possibly due to fabrication error. The bandwidths at the low and high frequency bands are 80 and 255 MHz, respectively.

C. Radiation Patterns

Simulated (XFDTD) radiation patterns of the proposed antenna in the presence of the SAM phantom are shown in Fig. 6(a) and (b). The parasitic ILA increases the antenna gain both at 900 and 1880 MHz in the upper hemisphere in the region $\theta = 0° - 90°$. Peak antenna gain at 900 MHz is 0.6 dBi with the ILA as opposed to -2.3 dBi without the ILA. Similarly, at 1880 MHz, the peak gain are 2.8 and 2.6 dBi with and without the ILA, respectively.

V. Conclusion

A new concept to reduce the SAR and increase antenna radiation efficiency is investigated where, by adding a variable length dual-band parasitic ILA, the current distribution on the ground plane of a mobile wireless terminal is controlled. By controlling the current distribution, significant reduction in SAR and increase in antenna efficiency are obtained. Simulation results confirm that a dual-band parasitic ILA can significantly reduce the peak SAR at 900 and 1880 MHz when it is placed close to a dual-band PIFA on a ground plane. Radiation efficiencies of up to 49% and 55% can be achieved at 900 and 1880 MHz, respectively, when the proposed antenna is placed next to a homogeneous head phantom. Higher radiation efficiency will result in longer battery life, which is highly desirable for mobile terminals.

References

[1] J. Wang and O. Fujiwara, "Reduction of electromagnetic absorption in the human head for portable telephones by a ferrite sheet attachment," *IEICE Trans. Commun.*, vol. E80B, no. 12, pp. 1801–1815, Dec. 1997.

[2] J. Hwang and F. Chen, "Reduction of the peak SAR in the human head with metamaterials," *IEEE Trans. Antennas Propag.*, vol. 54, no. 12, pp. 3763–3770, Dec. 2006.

[3] S. Kwak, D. Smith, J. Kwon, and H. Choi, "Experimental tests of SAR reduction on mobile phone using EBG structures," *Electron. Lett.*, vol. 44, no. 9, pp. 568–569, Apr. 2008.

[4] R. F. J. Broas, D. F. Sievenpiper, and E. Yablonovitch, "A high-impedance ground plane applied to a cellphone handset geometry," *IEEE Trans. Microw. Theory Tech.*, vol. 49, no. 7, pp. 1262–1265, Jul. 2001.

[5] M. Sager, M. Forcucci, and T. Kristensen, "A novel technique to increase the realized efficiency of a mobile phone antenna placed beside a head-phantom," in *Proc. IEEE Antennas Propag. Soc. Int. Symp.*, Jun. 2003, vol. 2, pp. 1013–1016.

[6] J. Jung, S. Kim, K. Kong, J. Lee, and B. Lee, "Designing ground plane to reduce hand effects on mobile handsets," in *Proc. IEEE Antennas Propag. Soc. Int. Symp.*, Jun. 2007, pp. 1040–1043.

[7] Y. Okada, M. Yamamoto, and T. Nojima, "Unbalanced fed dipole antenna mounted on ground plane with L-shaped parasitic elements for mobile handsets," presented at the ISAP Int. Symp. Antennas Propag., Taipei, Taiwan, Oct. 27–30, 2008, Paper 1645395.

[8] J. Holopainen, J. Ilvonen, O. Kivekas, C. Ichelen, and P. Vainikainen, "Near field control of handset antennas based on inverted-top wavetraps: Focus on hearing-aid compatibility," *IEEE Antennas Wireless Propag. Lett.*, vol. 8, pp. 592–595, 2009.

[9] M. R. Islam and M. Ali, "Elevation plane beam scanning of a novel parasitic array radiator antenna for 1900 MHz mobile handheld terminals," *IEEE Trans. Antennas Propag.*, vol. 58, no. 10, pp. 3344–3352, Oct. 2010.

[10] "Ansoft Corporation," Canonsburg, PA [Online]. Available: http://www.ansoft.com

[11] *Recommended Practices for Determining the Peak Spatial-Average Specific Absorption Rate (SAR) in the Human Head for Wireless Communications Devices: Measurement Techniques*, IEEE P1528/D1.2, Working Group 1 of Subcommittee 2 of IEEE Standards Coordinating Committee 34, 2003.

[12] "Remcom, Inc.," State College, PA [Online]. Available: http://www.remcom.com

[13] P. Vainikainen, J. Ollikainen, O. Kivekäs, and I. Kelander, "Resonator-based analysis of the combination of mobile handset antenna and chassis," *IEEE Trans. Antennas Propag.*, vol. 50, no. 10, pp. 1433–1444, Oct. 2002.